ELSEVIER

Nuclear Physics A 614 (1997) 112–128

NUCLEAR PHYSICS A

Study of polarized ^{7}Li scattering from ^{208}Pb at 33 MeV

K. Rusek [a], J. Gómez-Camacho [b], I. Martel-Bravo [b], G. Tungate [c]

[a] *Soltan Institute for Nuclear Studies, Hoza 69, 00-681 Warsaw, Poland*

[b] *Departamento de Física Atómica, Molecular y Nuclear, Universidad de Sevilla, 41080 Sevilla, Spain*

[c] *School of Physics and Space Research, The University of Birmingham, Birmingham B15 2TT, UK*

Received 1 October 1996

Abstract

Elastic and inelastic scattering of polarized ^{7}Li from ^{208}Pb at 33 MeV is investigated by means of the continuum-discretized coupled channel method, using diagonal and coupling potentials derived from empirical α, t-target optical model potentials. The effects of the projectile breakup into $\alpha + t$ as well as target excitation and one-neutron transfer reaction are studied. A good description of the experimental data is obtained. The scattering of ^{7}Li from ^{208}Pb at 33 MeV is found to be of similar nature to the scattering of ^{6}Li from the same target and at the same energy.

PACS: 25.70.Bc; 25.70.Hi

Keywords: NUCLEAR REACTIONS ^{208}Pb(polarized ^{7}Li,^{7}Li)^{208}Pb, E_x = 0.0, 0.478, 2.615 MeV, ^{208}Pb(polarized ^{7}Li,^{6}Li)^{209}Pb, E_{lab} = 33 MeV; CDCC and CRC analysis

1. Introduction

Effects of the strong coupling of the elastic to the inelastic and transfer channels are known to be very important at energies close to the Coulomb barrier. Optical Model (OM) calculations for the ^{16}O+^{208}Pb elastic scattering [1], with the bare potential obtained from folding nucleon–nucleon interactions of M3Y type with the projectile and target nucleon densities, overestimated the cross section data to large extent. An extensive coupled reaction channel (CRC) study of this scattering, which included projectile and target excitations as well as transfer reactions, led to a good description of the experimental elastic scattering data. The effective polarization potential derived from the CRC calculations was attractive and energy dependent.

Analyses of elastic scattering of weakly bound nuclei like ^{6,7}Li or ^{9}Be led to the conclusion that the polarization potential associated with the projectile breakup in the

PII S0375-9474(96)00449-6

field of the target nucleus is repulsive [2–4]. OM analyses of ^{7}Li scattering on many target nuclei [2,5–8] with the diagonal potentials obtained from a double folding (DF) model have shown that the experimental data could be reproduced with a reduced strength of the real folding potential. Analyses of ^{7}Li scattering, by coupled channel calculations (CC) which included $^{7}\mathrm{Li} \rightarrow \alpha + t$ sequential breakup via the resonant $7/2^-$ state at 4.63 MeV and the $5/2^-$ state at 6.68 MeV, partly accounted for this reduction [2,5–7]. The role of the ^{7}Li direct breakup via its nonresonant continuum was also investigated by means of the continuum-discretized coupled channel method (CDCC) and the effect of coupling to the nonresonant states was found to be of the same nature as for the sequential breakup [2,9].

Recently [10], data on the elastic scattering of ^{6}Li and ^{7}Li by ^{208}Pb were taken to investigate the scattering behaviour of these projectiles near the Coulomb barrier. Analyses of the data by means of OM with DF potentials indicated that the polarization potential for ^{6}Li remains repulsive for all energies, while for ^{7}Li the potential changes sign and is attractive, as for ^{16}O, at near barrier energies. This change affects both the central and tensor parts of the potential, and is consistent with dispersion relations [11]. This finding suggested that some processes other than projectile breakup may dominate at the barrier. One-neutron transfer was among the most obvious candidates. However, a detailed study using polarized ^{7}Li beam and analysis of the data by means of CRC method [12] could not explain this anomaly. In the analysis projectile excitation to its low-lying resonant states as well as one-neutron transfer channels were included. Although the inclusion of the transfer channels induced an effect equivalent to the attractive polarization potential, the final results of the calculations still overestimated by far the values of the differential cross section for ^{7}Li+^{208}Pb elastic scattering.

The current paper is devoted to a more comprehensive study of the anomalous ^{7}Li+^{208}Pb elastic scattering in the vicinity of the Coulomb barrier. The existing set of experimental data at an incident energy of 33 MeV for elastic scattering, excitation of the projectile to its first excited state at 0.48 MeV, excitation of the target to the 3^- vibrational state at 2.165 MeV and one-neutron transfer data, are reanalyzed by means of CDCC and CRC calculations. The effects of the $^{7}\mathrm{Li} \rightarrow \alpha + t$ sequential and direct breakup on the elastic scattering channel are studied. Although ^{7}Li scattering was investigated by CDCC calculations [2,9], effects of transfer channels on such calculations were never investigated. The inelastic scattering data corresponding to the target excitation are presented here for the first time. The calculations are performed with a bare potential obtained from folding α+^{208}Pb and t+^{208}Pb phenomenological optical model potentials using ^{7}Li cluster wave functions. This semi-empirical approach is compared with the results of the previous analysis [12] performed using DF potentials.

2. The calculations

The calculations were performed using the CRC code Fresco (version FRXP) [13]. The coupled equations were integrated up to 40 fm, with step size 0.1 fm, and up to

65 partial waves were used. Couplings were included between ^{7}Li= $\alpha + t$ cluster states: the ground state, the excited state at excitation energy of 0.48 MeV, the resonant states at excitation energies of 4.63 MeV and 6.68 MeV and nonresonant continuum states.

The nonresonant continuum states were treated in line with the model of Sakuragi et al. [2,9]. The $\alpha + t$ continuum over the breakup threshold was discretized into momentum bins with respect to the momentum $\hbar k$ of the $\alpha - t$ relative motion. The width of a bin was set to $\Delta k = 0.25$ fm^{-1}. The cluster wave functions for each bin were averaged over the bin width and the resulting wave function was normalized to unity. Each bin was then treated as an excited state of ^{7}Li with excitation energy corresponding to the mean bin energy. The spin of the state $\boldsymbol{I}$ was found from the vector sum over the $\alpha - t$ relative angular momentum $\boldsymbol{L}$ and triton spin s. The ^{7}Li+^{208}Pb scattering wave functions were calculated at the mean bin energy and assumed to be energy independent within the bin.

The CDCC analysis of ^{7}Li breakup, into an α particle plus triton by a ^{120}Sn target, brought an important finding [14]. The contribution of the $L = 0$ bin to the breakup cross section was large, but the coupling to this bin did not affect the elastic scattering channel. Test calculations for ^{7}Li+^{208}Pb confirmed this finding. Although the calculated total breakup cross section was dominated by the $L = 0$, $0.0 \leq k \leq 0.25$ fm^{-1} bin, the influence of this bin on the elastic scattering was negligible. Odd parity $L = 1, 3$ bins at higher excitation energies affected the elastic channel more seriously. This is because the breakup via the $L = 0$, $0.0 \leq k \leq 0.25$ fm^{-1} bin dominates at scattering angles where the elastic scattering cross section is large and therefore less sensitive to couplings to breakup channels. At backward scattering angles, where the elastic scattering cross section is small, the $L = 0$ bin contributes to the breakup cross section much less than the odd parity bins. Therefore its influence on the elastic channel is very small. This is illustrated in Fig. 1 where results of two-channel (2ch) calculations which included ground and first excited states of ^{7}Li are compared with results of CDCC calculations where an additional nonresonant continuum state was included. Inclusion of the $L = 0$, $I = 1/2^+$ bin located at an excitation energy of 0.38 MeV above the breakup threshold affected the elastic scattering cross section much less than the inclusion of $L = 1$, $I = 3/2^-$ bin at $E_x = 1.9$ MeV. In the lower part of Fig. 1 the calculated angular distributions of the differential breakup cross section for these bins are shown. Note that the cross section for the $L = 0$ bin shown by the dotted curve is much larger than that for the $L = 1$ bin.

The $L = 2$ continuum showed a similar behaviour to the $L = 0$ component in that its effect on the breakup was significant although coupling to it had little impact on the description of the elastic scattering data. Since the emphasis of the present analysis is on the elastic scattering channel, the values of the $\alpha - t$ relative angular momentum were limited to $L = 1, 3$.

A number of test calculations were carried out in order to determine the truncation of the $\alpha + t$ continuum. It was found that the continuum states can be limited to $0.25 \leq k \leq 0.75$ fm^{-1} for the present purpose. Detailed calculations which included all $L = 1$ and $L = 3$ states have shown that the effect of the $0.0 \leq k \leq 0.25$ fm^{-1} bin as well as

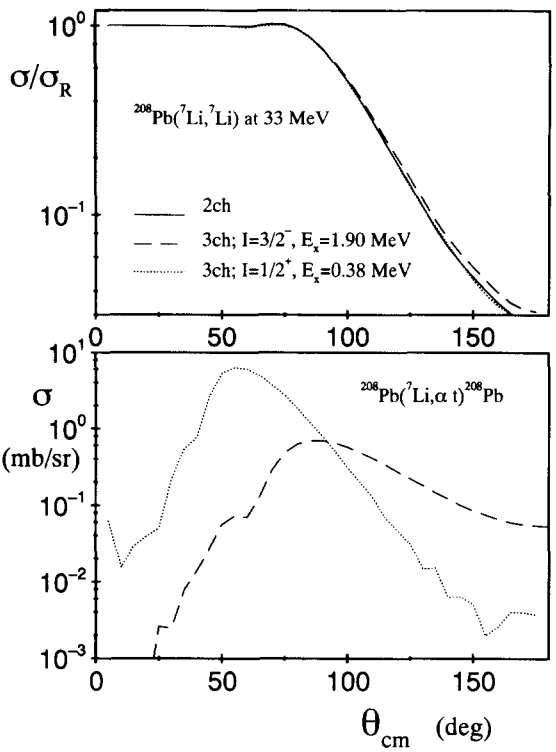

Fig. 1. Influence of the $L = 0, 1$ bins on the elastic scattering channel is shown in the upper part of the figure. The solid curve shows results of CC calculations which included the ground and the first excited states of ^{7}Li. The dotted curve shows an effect of the $L = 0$, $I = 1/2^+$ bin located at an excitation energy of 0.38 MeV above the breakup threshold while the dashed curve shows an effect of the $L = 1$, $I = 3/2^-$ bin at 1.90 MeV. In the lower part of the figure the $^7\text{Li} \rightarrow \alpha + t$ breakup cross sections for the $L = 0$ and $L = 1$ bins are plotted.

$0.75 \leq k \leq 1.0$ fm^{-1} bin on the elastic scattering channel is negligible. Thus, in order to limit number of channels involved in the analysis, those bins were neglected in the calculations. The excited states of ^{7}Li used in the analysis are listed in Table 1.

2.1. *Cluster-folding potentials*

The diagonal and coupling potentials were calculated from phenomenological $\alpha-^{208}$Pb (V_α) and $t-^{208}$Pb (V_t) OM potentials using the cluster-folding (CF) method,

$$V_{if}(R) = \langle \Psi_f(r) | V_t(|\boldsymbol{R} + \tfrac{4}{7}\boldsymbol{r}|) + V_\alpha(|\boldsymbol{R} - \tfrac{3}{7}\boldsymbol{r}|) | \Psi_i(r) \rangle , \quad (1)$$

where $\boldsymbol{R}$ is the ^{7}Li-target separation and $\boldsymbol{r}$ is the separation between the clusters. The input t, α-target OM potentials should be taken at $\frac{3}{7}$ and $\frac{4}{7}$ of the incident ^{7}Li energy, respectively. In the analysis an $\alpha+^{208}$Pb OM potential [15], found in a near Coulomb barrier study, and a global $t+^{208}$Pb potential [16], describing triton scattering at energies 15–20 MeV, were used. The parameters of these potentials are listed in Table 2.

The real part of the diagonal CF potential for ^{7}Li+^{208}Pb is represented by the solid

Table 1
Model space for ^{7}Li. The energies E_{min} and E_{max} are limits of a continuum bin and E_x is its mean energy, relative to the $^7Li \rightarrow \alpha + t$ breakup threshold. In the last column the calculated cross section is listed.

L	I^π	E_x [MeV]	E_{min} [MeV]	E_{max} [MeV]	σ [mb]
1	$3/2^-$	−2.47	–	–	721.9 [a]
1	$3/2^-$	1.90	0.76	3.04	3.0
1	$3/2^-$	4.94	3.04	6.84	0.5
1	$1/2^-$	−1.99	–	–	35.8
1	$1/2^-$	1.90	0.76	3.04	1.6
1	$1/2^-$	4.94	3.04	6.84	0.2
3	$7/2^-$	2.16	–	–	1.6
3	$7/2^-$	4.94	3.04	6.84	0.5
3	$5/2^-$	4.21	1.71	6.71	0.2

[a] Total reaction cross section.

Table 2
Parameters of the optical model potentials

	V (MeV)	r_0 (fm)	a_0 (fm)	W (MeV)	r_i (fm)	a_i (fm)	r_C (fm)
α+^{208}Pb [a]	35.0	1.547	0.570	9.0	1.547	0.570	1.547
t+^{208}Pb [b]	161.24	1.20	0.720	18.06	1.40	0.84	1.30
n+^{6}Li [c]	BE[f]	1.25	0.65				
n+^{208}Pb [d]	BE[f]	1.25	0.65				
^{6}Li+^{209}Pb [e]	109.5	1.326	0.811	22.39	1.534	0.884	1.30

[a] Ref. [15].
[b] Ref. [16].
[c] Ref. [17].
[d] Ref. [18].
[e] Ref. [19].
[f] The depth of the potential was adjusted in order to obtain the correct binding energy of a particular state.

curve in Fig. 2. The potential is very similar to the CF potential used in analysis of ^{6}Li+^{208}Pb scattering at the same incident energy of 33 MeV [20] (dashed curve in Fig. 2). Note that the DF potential used in OM analysis of ^{7}Li+^{208}Pb elastic scattering [10] is twice as deep as the CF one. However, in the surface region the CF potential is stronger than that of the DF model.

2.2. *Cluster wave functions*

Cluster wave functions of ^{7}Li, recently used in a study of ^{7}Li breakup into an α particle and a triton on a ^{120}Sn target [14], were adopted in the present analysis. They were calculated in a Woods–Saxon (WS) potential well having geometry parameters R = 2.20 fm and a = 0.70 fm (Table 3). The wave functions were tested in CC calculations for polarized ^{7}Li+^{120}Sn scattering at 44 MeV and polarized ^{7}Li+^{58}Ni scattering at 20.3 MeV. In these calculations couplings to the first excited and two resonant states of ^{7}Li were involved. The parameters of the input potentials were the

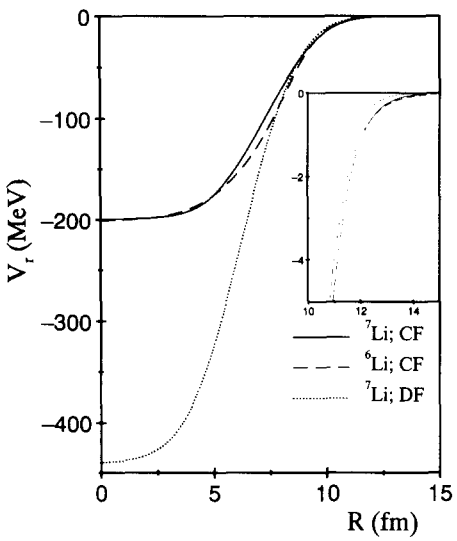

Fig. 2. Real parts of the central potentials for ^{6,7}Li + ^{208}Pb scattering at 33 MeV. The CF potential for ^{7}Li shown by solid curve is used in this paper, the DF potential shown by the dotted curve was used in the analysis presented in Ref. [10] while the CF potential for ^{6}Li was used in Ref. [20].

Table 3
Reduced transition probabilities and spectroscopic quadrupole moment of ^{7}Li calculated for different geometries of the $\alpha - t$ binding potential together with the experimental values

	Q_S (e·fm^2)	B(E2; $3/2^- \rightarrow 1/2^-$) e^2fm^4	B(E2; $3/2^- \rightarrow 7/2^-$) e^2fm^4	B(E2; $3/2^- \rightarrow 5/2^-$) e^2fm^4
R = 2.20 fm	−3.71	7.29	10.44	0.47
R = 2.05 fm	−3.58	6.81	9.48	1.19
R = 1.80 fm	−3.39	6.11	8.14	2.35
B-M	−3.83	7.75	11.75	1.09
exp.	−4.00 [a]	7.27 [a]	17.5 [b]	3.4 [b]

[a] Ref. [23].
[b] Ref. [24].

same as in Refs. [6,21,22]. The final results of the calculations were very close to those obtained in the previous studies [6,21,22].

The results of the CDCC calculations for ^{7}Li+^{208}Pb depend on the geometry of the potential binding the α and t clusters into ^{7}Li. Test calculations were performed, including ^{7}Li bound, resonant and nonresonant continuum states as listed in Table 1, in order to study this dependence. Several commonly used $\alpha - t$ binding potentials were tested. The results for elastic scattering are plotted in Fig. 3.

Using the geometry parameters R = 2.20 fm and a = 0.70 fm the correct value of the reduced transition probability between the ground and the first excited state can be obtained (Table 3). CDCC calculations with this binding potential are shown by the solid curves in Fig. 3.

The calculations using a binding potential with a WS shape with a = 0.7 fm and

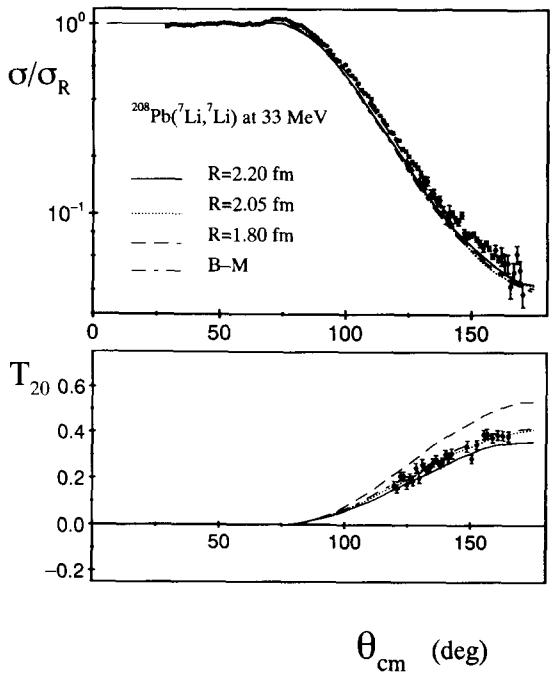

Fig. 3. Results of the CDCC calculations for the elastic channel using different $\alpha - t$ binding potentials (see text). The calculations included the elastic channel, ^{7}Li excitation to its first excited state, two resonances at excitation energies of 4.63 and 6.68 MeV relative to the ground state and five continuum bins as listed in Table 1. The experimental data are from Refs. [10,11].

$R = 2.05$ fm, as proposed by Kubo and Hirata [25] and extensively used in the analyses of polarized ^{7}Li scattering [21,22,26], are displayed by the dotted curves. The calculated values of the spectroscopic quadrupole moment (Q_S) and $B(E2; 3/2^- \rightarrow 1/2^-)$ are smaller than the experimental ones [23].

CDCC calculations using a WS geometry with $R = 1.8$ fm and $a = 0.7$ fm [27,28] for the binding potential produced very large values for the second rank tensor analyzing power (TAP) T_{20} as shown by dashed curve in Fig. 3. Calculated values of the Q_S and of the reduced transition probabilities are too small.

The last tested $\alpha - t$ binding potential was that of Buck and Merchant [29], which had a Gaussian shape. Values of the differential cross section and TAP for the elastic channel obtained with this potential (dot-dashed curves in Fig. 3) are very close to the results with the geometry $R = 2.05$ fm, $a = 0.7$ fm. The value of the spectroscopic quadrupole moment corresponding to this potential is closest to the experimental value but the reduced transition probability $B(E2; 3/2^- \rightarrow 1/2^-)$ is somewhat overestimated.

Results discussed in the next chapter were obtained with the geometry $R = 2.20$ fm and $a = 0.70$ fm.

Simple one-channel calculations, with ^{7}Li ground state reorientation, showed that the value of T_{20} scaled with the value predicted for Q_S. This relation was lost by inclusion of more coupled channels. CC calculations which included couplings to the resonant

Table 4
Calculated values of the elastic scattering $T_{20}(170°)$ for different numbers of coupled channels and for different $\alpha - t$ binding potentials

	Q_S (e·fm^2)	1ch	4ch	9ch
B–M	−3.83	0.543	0.504	0.414
R = 2.20 fm	−3.71	0.535	0.479	0.357
R = 2.05 fm	−3.58	0.525	0.475	0.402
R = 1.80 fm	−3.39	0.508	0.482	0.564

and nonresonant projectile states generated the largest values of T_{20} with the binding potential having geometry R = 1.8 fm, a = 0.7 fm (see Fig. 3). This potential, however, gave the lowest value of the Q_S. Calculated values of the second rank TAP, T_{20}, at a scattering angle of 170^o are listed in Table 4 for different numbers of coupled channels and different binding potentials. One-channel calculations included reorientation of the ^{7}Li ground state, four-channel calculations included couplings to the first excited and two resonant states while nine-channel calculations included couplings to all the states listed in Table 1. Generally, reorientation of the ^{7}Li ground state produced large values of the T_{20} which were reduced by inclusion of projectile excitations to its resonant and nonresonant states. One exception from this rule occurred for the potential having parameters R = 1.80 fm, a = 0.70 fm, for which couplings to the projectile nonresonant excited states increased calculated values of T_{20}.

3. Results

Simple OM calculations with a CF potential significantly underestimated the differential cross section for the ^{7}Li+^{208}Pb elastic scattering and were unable to generate nonzero second rank TAP. In order to achieve a good description of the differential cross section data, the real CF potential had to be multiplied by a reduction factor of 0.56. The OM results are compared to the experimental data in Fig. 4. Previous OM calculations [12] with the real part of the diagonal potential obtained from DF model overestimated the experimental data to large extent.

This disagreement can be explained by comparison of the real parts of the two potentials used – CF and DF as shown in Fig. 2. The DF potential for ^{7}Li+^{208}Pb at 33 MeV is much deeper than the CF one, but at the radius of strong absorption, 12.51 fm [10] for this system, the CF potential is almost twice as attractive as the DF one (see the inset to Fig. 2). Multiplying the strength of the real part of the DF potential by the ratio of the CF to DF potential values taken at 12.51 fm, which is 1.89, and performing OM calculations with such artificially changed DF potential we obtained result close to that calculated with the CF potential. A comparison of the OM calculations with the CF, DF and DF multiplied by the factor 1.89 potentials is presented in Fig. 5.

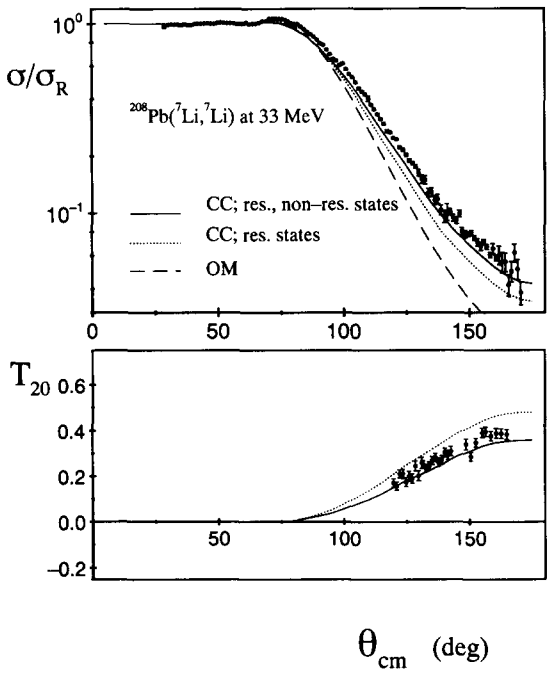

Fig. 4. Angular distributions of the differential cross section and second rank TAP T_{20} for the elastic channel. The dashed curve shows results of OM calculations with a CF central potential, the dotted curves are results of CC calculations which included couplings to the first excited and two resonant states of the projectile. The solid curves represent results obtained including all the states listed in Table 1.

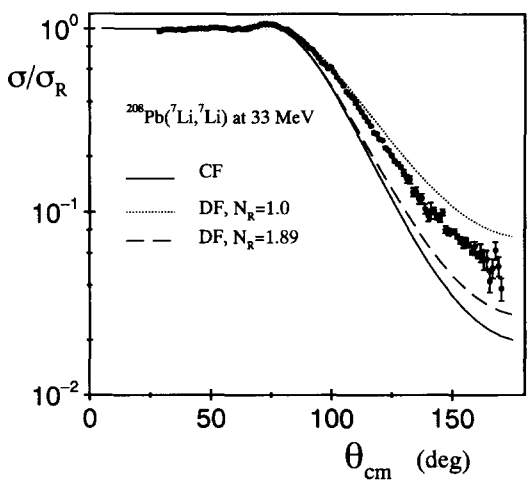

Fig. 5. Results of OM calculations using different potentials. The solid curve corresponds to the calculations with the CF potential, the dotted with the DF potential used previously [12] and the dashed curve with the real part of the DF potential renormalized by a factor of 1.89.

3.1. Projectile excitation

When the projectile excitations to the bound and two resonant states were included, the calculated values of the differential cross section and T_{20} became much closer to the data, as shown by dotted curves in Fig. 4. The calculations also correctly reproduced the angular distributions of the differential cross section and TAP for the inelastic scattering, leading to the $1/2^-$ excited state (Fig. 6). Inclusion of the nonresonant continuum, using truncation and discretization of the model space as shown in Table 1, farther improved the description of the data in the elastic channel (solid curves in Fig. 4).

Generally, the effect of projectile excitation including $^7\mathrm{Li} \rightarrow \alpha + t$ sequential breakup via resonant states as well as direct breakup via nonresonant continuum states had a large impact on the ^{7}Li+^{208}Pb elastic scattering. It increased the calculated values of the differential cross section for this system and generated TAPs. Similar conclusions could be drawn from the CC calculations with the DF potential performed previously [12].

In order to check if the projectile excitation effect could be compared to an effect of a repulsive polarization potential, as discussed for ^{6}Li+^{208}Pb scattering [3], OM calculations were performed with independently varied renormalizations for the real and imaginary parts of the central CF potential. An angular distribution of the differential cross section which was very close to that emerging from the CC calculations, shown by the solid curve in Fig. 4, was obtained with the renormalization parameters $N_r = 0.6$ for the real part and $N_i = 1.2$ for the imaginary part of the central potential. Thus, this indicates that the projectile excitation effect can be simulated by a repulsive real polarization potential. However, a correction of the imaginary part of the central potential is also required. The OM calculations with the renormalized central potential, however, do not generate any TAPs.

3.2. Comparison with the rotational model approximation

In some of the previous analyses of ^{7}Li scattering by means of CC calculations the quadrupole coupling formfactors were calculated assuming a simple rotational model for ^{7}Li. The ground and the first excited states of ^{7}Li, including resonances at 4.63 MeV and 6.68 MeV of excitation energy, were assumed to be members of $K = 1/2$ ground state rotational band [7,12]. Since one of the motivations of the present calculations was a comparison not only with the data but also with the previous analysis [12], it was of interest to check how these results were influenced by the rotational model approximation.

In order to do this, CC calculations were performed, which included couplings to the first excited and two resonant states of ^{7}Li. The coupling formfactors were calculated from the CF diagonal potential using rotational model wave functions as described in [12]. The reduced matrix element for the Coulomb excitation was set to 6.03 $e\cdot\mathrm{fm}^2$, the value used previously [12]. The deformation length, equal for the real and imaginary parts of the coupling formfactors, was found from the fit to the absolute values of the differential cross section in the inelastic channel. As a result, the value of the deformation

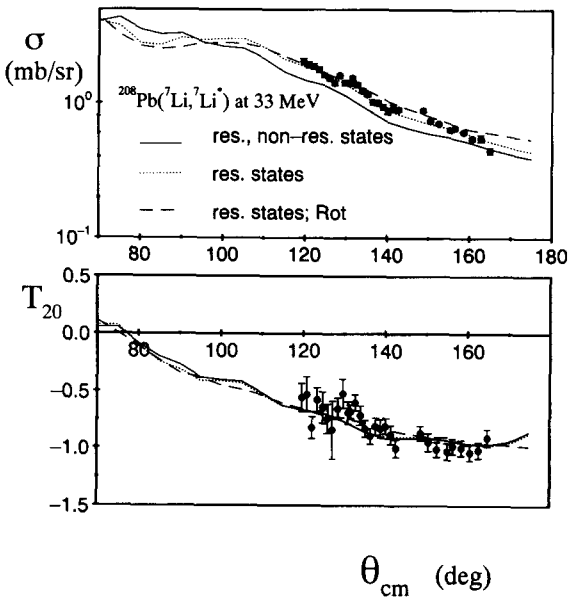

Fig. 6. Angular distributions of the differential cross section and second rank TAP for the inelastic channel. The experimental data are from Ref. [11]. The solid and dotted curves correspond to the calculations as in Fig. 4. The dashed curves represent CC calculations which included couplings to the first excited state and two resonant states of ^{7}Li with formfactors calculated using the rotational model for this nucleus.

length used in the calculations was 1.70 fm, significantly larger than the 1.12 fm used previously [12].

The results of the CC calculations with the rotational model formfactors described the experimental data for ^{7}Li+^{208}Pb inelastic scattering only slightly worse than the calculations with the CF formfactors, as shown in Fig. 6 by the dashed and dotted curves, respectively. However, the effect of the projectile excitation on the elastic scattering cross section (taken with respect to the OM calculation), emerging from the CC calculation with the rotational model formfactors, was much larger than the effect estimated by the calculation with the CF formfactors. This difference is much less pronounced for the second rank TAP. The comparison between these two calculations is presented in Fig. 7.

Summarizing, the test calculations suggest that the use of the rotational model formfactors may lead to an overestimation of the effect of $^7\mathrm{Li} \rightarrow \alpha + t$ sequential breakup on the elastic scattering cross section at backward scattering angles.

3.3. Target excitation

A set of the experimental data for ^{208}Pb excitation to its 3^- first excited state at excitation energy of 2.615 MeV was obtained simultaneously with the ^{7}Li+^{208}Pb elastic scattering data [11] but not published yet. The data are plotted in Fig. 8. The cross section for this process is smaller than for the ^{7}Li excitation to its first excited state and the values of the second rank TAP are of opposite sign to those for the projectile

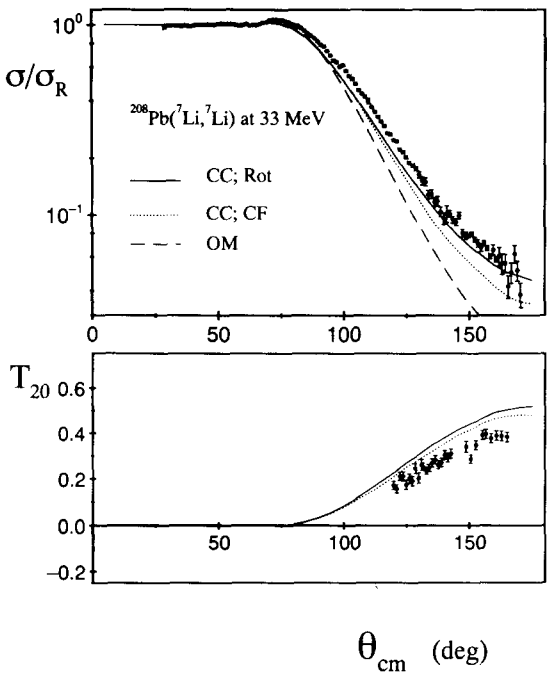

Fig. 7. Results of the four-channel calculations, which included couplings to the first excited and two resonant states of ^{7}Li, with coupling formfactors obtained from CF (dotted curves) and rotational (solid curves) models. The OM results are also shown for reference (dashed curve).

excitation. In fact, they are quite similar to those for the elastic data.

The optical α-target and t-target potentials, used to derive the CF ^{7}Li–target potential, were complex and accounted for the effects due to α and t internal structures as well as for the internal structure of the target nucleus. Thus, there is a danger that including target excitation in the ^{7}Li+^{208}Pb scattering analysis, one may account twice for the same effect. On the other hand, it is interesting to see if the effect of the target excitation is of the similar nature as the projectile excitation effect.

In the present calculations the target excitation was included in a very approximate way. The ^{208}Pb excited state was treated as a collective state and the coupling formfactor to this state was chosen to be a derivative of the CF diagonal potential [30]. The deformation lengths for the real and imaginary parts were set to be equal, $\delta_r = \delta_i = \delta =$ 0.7 fm. The value of δ was derived from the known experimental value of the reduced transition probability $B(\mathrm{E3}; 0^+ \rightarrow 3^-) = 0.621\ \mathrm{e^2b^3}$ [31] using the expressions given in Ref. [30]. It is in good agreement with that previously used [1,31]. The Coulomb coupling potential had a standard form [12] with the reduced matrix element calculated from the experimental value of the reduced transition probability.

In the calculations any effects due to a mutual excitation of both the projectile and the target were not included.

The CC calculations which included ground, first excited and two resonant states of ^{7}Li underestimated the differential cross section for the ^{208}Pb(^{7}Li,^{7}Li)^{208}Pb* inelastic

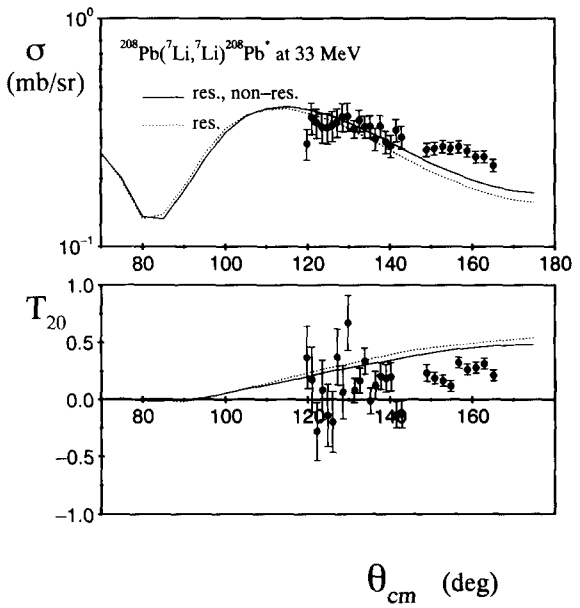

Fig. 8. Calculations for the inelastic scattering leading to the ^{208}Pb excitation to its first excited state at 2.615 MeV. The curves correspond to the projectile excitation as in Fig. 4.

scattering at backward angles and overestimated the values of T_{20} as shown by dotted curves in Fig. 8. Full CDCC calculations improved the description for both observables (solid curves) but still the data at backward angles were not well reproduced.

The effect of the inelastic scattering on the elastic cross section was found to be of the same nature as the effect of the projectile excitation. Inclusion of the target first excited state improved the description of the elastic scattering experimental data (dotted curves in Fig. 9). This effect is, however, much weaker than that of the projectile excitation.

3.4. Transfer channels

An effect of the one-neutron transfer reaction leading to a few low-lying states in ^{209}Pb on the ^{7}Li+^{208}Pb elastic scattering was found previously to be very important [12]. The strongest effect was associated with the transfers to the ground and $5/2^+$, 1.567 MeV, excited states of ^{209}Pb. In order to see if the effect of a transfer channel on the elastic scattering is of the same nature as reported previously [12], coupling to the one-neutron transfer reaction leading to the ^{209}Pb ground state was included in the present analysis.

Just as in the case of target excitation, there is a possibility that some part of the total transfer effect was already included in the imaginary part of the CF ^{7}Li+^{208}Pb central potential. Thus, the quantitative results of the present calculations may not be accurate. Nevertheless, they should exhibit the nature of the influence that transfer will have on the elastic channel.

In the calculations only one-neutron transfer from the ^{7}Li ground state to the ^{209}Pb

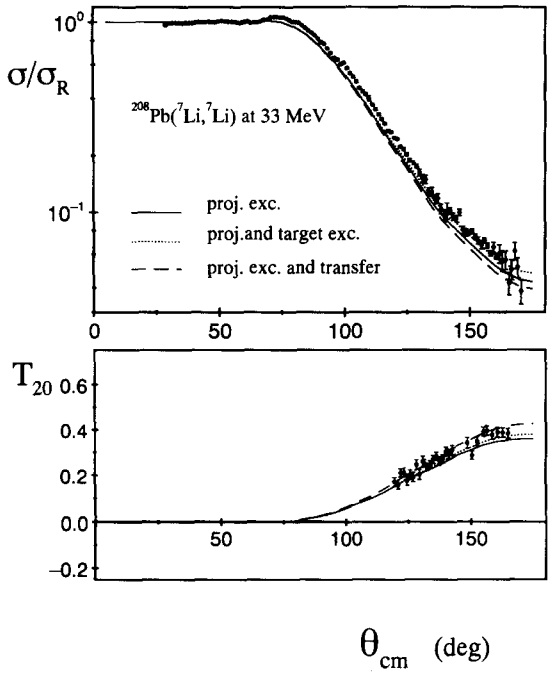

Fig. 9. Effects of the one-neutron transfer reaction (dashed curves) and the target excitation (dotted curves) on the elastic scattering. The solid curves correspond to the results shown in Fig. 4.

ground state was included. This was limited by computer capacity.

The parameters of the potentials binding the neutron to the ^{6}Li and ^{208}Pb cores as well as those describing the ^{6}Li+^{209}Pb exit channel were taken from the previous analysis [12] and are listed in Table 2. The spectroscopic factors for ^{7}Li = ^{6}Li + n were adopted from the shell model predictions of Cohen and Kurath [32], while the spectroscopic factor for ^{209}Pb = ^{208}Pb + n was set to unity as previously described [12].

The results of the calculations for the transfer reaction data are plotted in Fig. 10. In the calculations all the resonant and nonresonant excited states of the projectile as listed in Table 1 were included in the entrance channel, but excitation of the target nucleus was omitted. As shown in Fig. 10, the calculations reproduced very well the angular distribution of the second rank TAP and slightly underestimated the differential cross section values, which is very similar to the results of the CRC calculations performed previously [12].

The estimated effect of the one-neutron transfer reaction on the elastic scattering is shown by dashed curves in Fig. 9. Inclusion of this reaction channel reduced the differential cross section for the elastic scattering and increased the values of the T_{20} at backward angles. The observed effect is similar in its nature to the one found in the previous analysis [12].

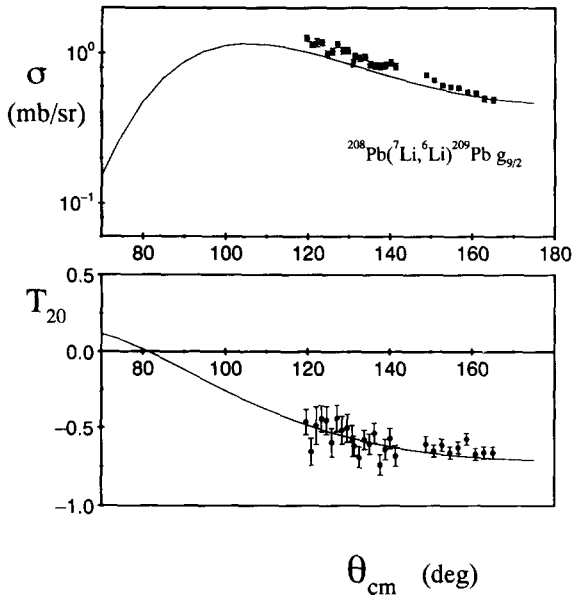

Fig. 10. Results of the calculations for the one-neutron transfer reaction leading to the ground state of ^{209}Pb. The experimental data are from Ref. [12].

4. Conclusions

A large amount of experimental data was analyzed in a consistent way by CC calculations with CF potentials. The most pronounced outgoing channels observed experimentally for the ^{7}Li+^{208}Pb interaction at 33 MeV were taken into account. The calculations reproduced all the experimental data without any adjustable parameters. All the parameters used as an input into the calculations, such as parameters of the OM potentials, spectroscopic factors, deformation lengths or reduced matrix elements, were adopted from relevant studies.

Special attention was paid to the projectile excitation process. It was found to play the most important role in the ^{7}Li+^{208}Pb interaction. Both types of excitations, the excitation to the bound excited state of ^{7}Li including ground state reorientation as well as excitation to the unbound resonant and nonresonant continuum states, affected the differential cross section for the elastic scattering in the same way. They increased the calculated values of the cross section. For the second rank TAP the common rule like for the cross section was not observed. The reorientation of the ^{7}Li ground state generated large values of the T_{20} which were next reduced by inclusion of couplings to the bound, resonant and nonresonant continuum states of the projectile.

The effect of the target excitation on the elastic scattering cross section was found to be of the same nature as that of projectile excitation. Inclusion of the ^{208}Pb excitation to its first excited state increased the differential cross section for the elastic scattering. The values of T_{20} were also slightly increased.

One-neutron transfer reaction had an opposite effect on the elastic scattering channel

to that of projectile excitation. Its inclusion reduced the values of the elastic scattering differential cross section and increased values of the TAP. A similar effect was found previously [12].

The massive CC calculations were not able to produce as good a description of the elastic scattering cross section data as the OM calculations with the real CF potential multiplied by a factor of 0.56. A reduction of the real part of the diagonal and coupling potentials by 10 percent and the imaginary part by 30 percent would result in a still better description of the differential cross section for the elastic channel. This could be interpreted as being due to the limited number of the nonresonant continuum states of the projectile taken into account in the calculations as well as an approximate treatment of the target excitation and the one-neutron transfer reaction.

Summarizing, the present analysis confirmed many of the observations made previously [12] like an "attractive nature" of the transfer reactions or a "repulsive nature" of the projectile excitation. The present calculations described the elastic scattering data much better without any renormalization of the CF potentials than the calculations performed with DF potentials. A need for a strong reduction of the CF central potential found in OM fit to the elastic scattering cross section data could be understood in terms of couplings to the inelastic and transfer channels.

CF and DF analyses are complementary to understand ^{7}Li scattering. CF is more successful than DF in giving parameter-free fits of the cross sections, and so it provides the relevant reaction mechanisms, at a given energy. However, CF potentials have to be obtained phenomenologically for each energy, while DF potentials are basically energy independent. Thus, DF analysis is more adequate to study the energy dependence of the reaction mechanisms [33].

Acknowledgements

This work was supported in part by the State Committee for Scientific Research (KBN) of Poland.

References

[1] I.J. Thompson, M.A. Nagarajan, J.S. Lilley and M.J. Smithson, Nucl. Phys. A 505 (1989) 84.
[2] Y. Sakuragi, M. Yahiro and M. Kamimura, Prog. Theor. Phys. Supp. 89 (1986) 136.
[3] Y. Sakuragi, Phys. Rev. C 35 (1987) 2161.
[4] Y. Hirabayashi, S. Okabe and Y. Sakuragi, Phys. Lett. B 221 (1989) 227.
[5] J. Gomez-Camacho, M. Lozano and M.A. Nagarajan, Phys. Lett. B 161 (1985) 39.
[6] Y. Sakuragi, M. Yahiro, M. Kamimura and M. Tanifuji, Nucl. Phys. A 462 (1987) 173.
[7] G. Tungate, D. Krämer, R. Butsch, O. Karban, K.-H. Möbius, W. Ott, P. Paul, A. Weller, E. Steffens, K. Becker, K. Blatt, D. Fick, B. Heck, H. Jänsch, H. Leucker, K. Rusek, I.M. Turkiewicz and Z. Moroz, J. Phys. G 12 (1986) 1001.
[8] C.W. Glover, R.I. Cutler and K.W. Kemper, Nucl. Phys. A 341 (1980) 137.
[9] Y. Sakuragi, M. Yahiro, M. Kamimura and M. Tanifuji, Nucl. Phys. A 480 (1988) 361.
[10] N. Keeley, N.M. Clarke, B.R. Fulton, G. Tungate, J.S. Lilley and M.A. Nagarajan, Nucl. Phys. A 571 (1994) 326.

[11] I. Martel-Bravo, C.O. Blyth, N.M. Clarke, P.R. Dee, B.R. Fulton, J.A.R. Griffith, S.J. Hall, N. Keeley, K. Rusek, G. Tungate, N.J. Davis, K.A. Connell, J.S. Lilley, M.W. Bailey, J. Gomez-Camacho, Nucl. Phys. A 582 (1995) 357.
[12] K. Rusek, C.O. Blyth, N.M. Clarke, P.R. Dee, B.R. Fulton, J.A.R. Griffith, S.J. Hall, N. Keeley, I. Martel-Bravo, G. Tungate, N.J. Davis, K.A. Connell, J.S. Lilley, M.W. Bailey and J. Gomez-Camacho, Nucl. Phys. A 575 (1994) 412.
[13] I.J. Thompson, Comp. Phys. Rep. 7 (1988) 167.
[14] N.J. Davis, C.H. Shepherd-Themistocleous, A.C. Shotter, T. Davinson, D.G. Ireland, K. Livingston, E.W. MacDonald, R.D. Page, P.J. Sellin, P.J. Woods, N.M. Clarke, G. Tungate, J.A.R. Griffith, S.J. Hall, O. Karban, I. Martel-Bravo, J.M. Nelson, K. Rusek and J. Gomez-Camacho, Phys. Rev. C 52 (1995) 3201.
[15] G.M. Hudson and R.M. Davis, Phys. Rev. C 9 (1974) 1521.
[16] F.D. Becchetti and G.W. Greenlees, Proc. 3rd Int. Sypm. Pol. Phenomena, Madison, 1970, H.H. Barschall and W. Haeberli, eds. (University of Wisconsin, 1971) p. 682.
[17] O. Karban, G. Kuburas, C.O. Blyth, H.D. Choi, N.J. Davis, S.J. Hall, S. Roman, G. Tungate and I.M. Turkiewicz, Nucl. Phys. A 535 (1991) 377.
[18] M.E. Franey, J.S. Lilley and W.R. Phillips, Nucl. Phys. A 324 (1979) 193.
[19] J. Cook, Nucl. Phys. A 388 (1982) 153.
[20] N. Keeley and K. Rusek, Phys. Lett. B 375 (1996) 9.
[21] H. Nishioka, J.A. Tostevin, R.C. Johnson and K.-I. Kubo, Nucl. Phys. A 415 (1984) 230.
[22] H. Ohnishi, M. Tanifuji, M. Kamimura and M. Yahiro, Phys. Lett. B 118 (1982) 16.
[23] H.-G. Voelk and D. Fick, Nucl. Phys. A 530 (1991) 475.
[24] R.M. Hutcheon and H.S. Caplan, Nucl. Phys. A 127 (1969) 417.
[25] K.-I. Kubo and M. Hirata, Nucl. Phys. A 187 (1972) 186.
[26] H. Ohnishi, M. Tanifuji, M. Kamimura and M. Yahiro, Nucl. Phys. A 415 (1984) 271.
[27] V.I. Kukulin, V.G. Neudatchin and Y.F. Smirnov, Nucl. Phys. A 245 (1976) 429.
[28] T. Davinson, V. Rapp, A.C. Shotter, D. Branford, M.A. Nagarajan, I.J. Thompson and N.E. Sanderson, Phys. Lett. B 139 (1984) 150.
[29] B. Buck and A.C. Merchant, J. Phys. G 14 (1988) L211.
[30] M.J. Smithson, J.S. Lilley, M.A. Nagarajan, P.V. Drumm, R.A. Cunningham, B.R. Fulton and I.J. Thompson, Nucl. Phys. A 517 (1990) 193.
[31] M.M. Gazzaly, N.M. Hintz, G.S. Kyle, R.K. Owen, G.W. Hoffmann, M. Barlett and G. Blanpied, Phys. Rev. C 25 (1982) 408.
[32] S. Cohen and D. Kurath, Nucl. Phys. A 101 (1967) 1.
[33] I. Martel, J. Gomez-Camacho, K. Rusek and G. Tungate, Nucl. Phys. A 605 (1996) 417.